

Optical monitoring and IDV analysis of the blazars S5 0716+714 and 3C 273

Xiao-Lan Liu, Yu-Hai Yuan and Hong-Ren Huang

Center for Astrophysics, Guangzhou University, Guangzhou 510006, China; yh_yuan@gzhu.edu.cn

Astronomy Science and Technology Research Laboratory of Department of Education of Guangdong Province, Guangzhou 510006, China

Received 2020 June 24; accepted 2020 November 8

Abstract S5 0716+714 and 3C 273 are frequently studied blazars, which show obvious optical variabilities with different timescales. Using the 1.0 m telescope at the Yunnan Observatory, we monitored the two sources. For S5 0716+714, we report 990 observations during the monitoring duration from JD 2458536 to JD 2458540. For 3C 273, there are 884 observations during the monitoring duration from JD 2458539 to JD 2458542. Based on those observations, we obtain the following results. (1) For S5 0716+714, there lie intra-day optical variabilities (IDVs), with timescales from 0.31 hours to 2.64 hours. For 3C 273, it is possible that there lie IDVs, with timescales from 0.36 hours to 0.49 hours. (2) The time delay of S5 0716+714 is $\tau_{RI} = 3.46$ min between R and I bands, and the time delay of 3C273 is $\tau_{IV} = 6.42$ min between I and V bands. (3) We find that, for S5 0716+714, there lies a suspected intra-day period, $P \approx 185.78$ min; for 3C 273, there lie intra-day periods, which are about ~ 60 min and ~ 80 min.

Key words: quasars: general — quasars: individual (S5 0716+714, 3C 273) — galaxies: photometry

1 INTRODUCTION

The radiation from an active galactic nucleus (AGN) is believed to be the result of accretion of mass by a supermassive black hole at the center of its host galaxy (Esposito et al. 2015). Blazars are typical radio loud AGNs, which can emit a wide-range of electromagnetic radiation from radio to γ -ray and can be enhanced by Doppler beaming.

Blazars can be divided into two subclasses: flat spectral radio quasars (FSRQs) and BL Lacs, which can be distinguished according to the equivalent width (EW) of emission lines or the location of the synchrotron peak frequency (ν_p). Generally, FSRQs have typical broad emission lines, with $EW > 5\text{ \AA}$, while BL Lacs have weak emission lines ($EW < 5\text{ \AA}$), or no emission lines (Sandrinelli et al. 2016; Urry & Padovani 1995; Ghisellini et al. 2011; Sbarato et al. 2012; Ghisellini & Tavecchio 2015).

Some models can be used to explain the emission mechanism of high-energy radiation, such as the synchrotron self-Compton model (SSC), the soft photons scattered up to the γ -ray region are from the synchrotron emissions in the jet (Maraschi et al. 1992; Bloom & Marscher 1996; Zdziarski & Krolik 1993).

Blazars exhibit some extreme properties, such as rapidly and violently optical variability, high polarization, non-thermal continuum spectrum, core dominance,

superluminal motion, strong gamma-ray emission, etc (Urry & Padovani 1995; Ulrich et al. 1997). Among them, the optical variabilities are typical features, with the timescales from minutes to years (e.g., Poon et al. 2009; Zhang et al. 2008; Fan 2005; Fan et al. 2009b; Fan et al. 2014). Based on these timescales, the optical variabilities can be divided into three types: intra-day variabilities (IDVs), short-term variabilities (STVs), and long-term variabilities (LTVs).

IDVs show the timescales from minutes to hours (Oke 1967; Miller 1975; Gupta et al. 2008; Fan et al. 2009b; Dai et al. 2009; Poon et al. 2009; Fan et al. 2014; Yuan et al. 2015a; Fan et al. 2019). Agarwal & Gupta (2015) reported that, in B , V , R , or I bands, the amplitudes of variability are up to 31% for 3C 454.3, and 9.2% for 3C 273 among 21 nights. Liu et al. (2019) reported that 3C273 quickly brightened by $\Delta m_R \approx 0.05 \pm 0.01$ mag within 26.6 min.

The phenomenon of IDVs can be explained as the external interstellar scintillation (ISS) effect caused by scattering from the interstellar plasma screen between the sources and the observers (Spangler et al. 1989; Dennett-Thorpe & de Bruyn 2002), the decaying shock in jet or the accretion disc instabilities (Marscher & Gear 1985; Marscher et al. 2008; Chakrabarti & Wita 1993; Mangalam & Wita 1993). The IDV results can help us to study the emission regions, the Doppler factor, and the

central black hole of blazars (e.g., Wagner & Witzel 1995; Ciprini et al. 2003, 2007; Kalita et al. 2015; Dai et al. 2015).

LTVs with the timescales in years can be explained as the precession in binary black hole systems (Aller et al. 1985; Marscher & Gear 1985; Begelman et al. 1980; Sillanpää et al. 1988; Camenzind & Krockenberger 1992; Rieger & Mannheim 2000, 2003; Valtonen et al. 2008).

Research of multi-band time delays can help us to study the emission properties and constrain the emission locations. There are some works about these studies (Poon et al. 2009; Zhang 2010; Wu et al. 2012; Man et al. 2016). For example, Zhang (2010) found that the soft X-ray variations were observed to lag the hard X-rays by about 1000 s in S5 0716+714. Man et al. (2016) found that the time delays were 1.308 ± 0.603 min between R and I bands, 1.445 ± 0.511 min between the B and I bands. Meng et al. (2017) reported the time delay of about 10 min between the light curves from the V and R bands. Rani et al. (2013) found that high energy (optical - GeV) flares propagate down to radio frequencies dependence on the frequency with a slope ~ 0.3 following at 65 days time delay, and found that the opacity was important to producing time delays between light curves at optically thin and thick wavelengths.

The relationships between the flux densities and spectral variations at different bands have often been studied (e.g., Xie et al. 1999; Xie et al. 2004; Ghosh et al. 2000; Mantovani et al. 2000; Collmar et al. 2000; Sambruna et al. 2001). Fan et al. (2009c) found that the strength of the flux variations in higher frequencies was higher than those in the lower frequencies, and found that there lied time delay between V and I bands. Zeng et al. (2018) analyzed the correlations between the spectral indices and V -band flux densities and found that the spectrum became bluer when the sources became brighter.

S5 0716+714 is one of the frequently studied BL Lac objects, which show extreme variability on time-scales from minutes to years in all observed wavelengths, from radio to X-rays. It is a good target of intra-day research and has been studied by many authors (Poon et al. 2009; Gupta et al. 2012; Bhatta et al. 2013; Man et al. 2016; Lee et al. 2016, etc). Rani et al. (2013) found that the long-term variability (~ 350 days) trend was superimposed with shorter time scales (~ 60 days) in the optical light curves. Agarwal & Gupta (2015) found that the amplitudes of flux variability were up to 13.5% for S5 0716+714 on intra-day time-scales at B , V , R or I bands. Agarwal & Gupta (2015) calculated a possible time-scale of variability ~ 1.2 hours at I and V bands based on the structure-function (SF) on 2012 Jan. 21.

This paper is arranged as follows. Section 2 gives the observations and data reductions. Section 3 describes the

optical variability. Finally, Section 4 discusses the results and draws conclusions.

2 OBSERVATIONS AND DATA REDUCTIONS

The observations of S5 0716+714 and 3C 273 were carried out using the 1.0m optical telescope at the Yunnan Astronomical Observatory, which is equipped with an Andor DW 436 2048 \times 2048 pixels CCD system. The field of view of the telescope is about $7.3' \times 7.3'$ for a focal reducer.

The bias images are taken at the beginning and the end of the night's observation. The flat-field images are taken at the dusk and dawn. The data reduction is carried out by the standard procedures of IRAF, which is based on the Linux system. Photometry is obtained after the bias, dark and flat-field corrections.

Given K , the number of comparison stars, for each of them (S_i , $i=1,2,\dots,K$), we calculate the i th target magnitude (m_i): $m_i = m_{i|o} + m_{i|c} - m_{i|oc}$, here $m_{i|oc}$ is the instrument magnitude of the comparison star, $m_{i|o}$ is the instrument magnitude of the target, $m_{i|c}$ is the standard comparison star magnitude. Considering the whole comparison stars, the target magnitude (m) can be calculated as $m = \frac{\sum_{i=1}^K m_i}{K}$ with a standard error $\sigma = \sqrt{\frac{\sum(m_i - m)^2}{K-1}}$.

The comparison stars of 3C 273 are collected from Smith et al. (1985). The comparison stars of S5 0716+714 are collected from Villata et al. (1998).

3 OPTICAL VARIABILITIES

1. S5 0716+714

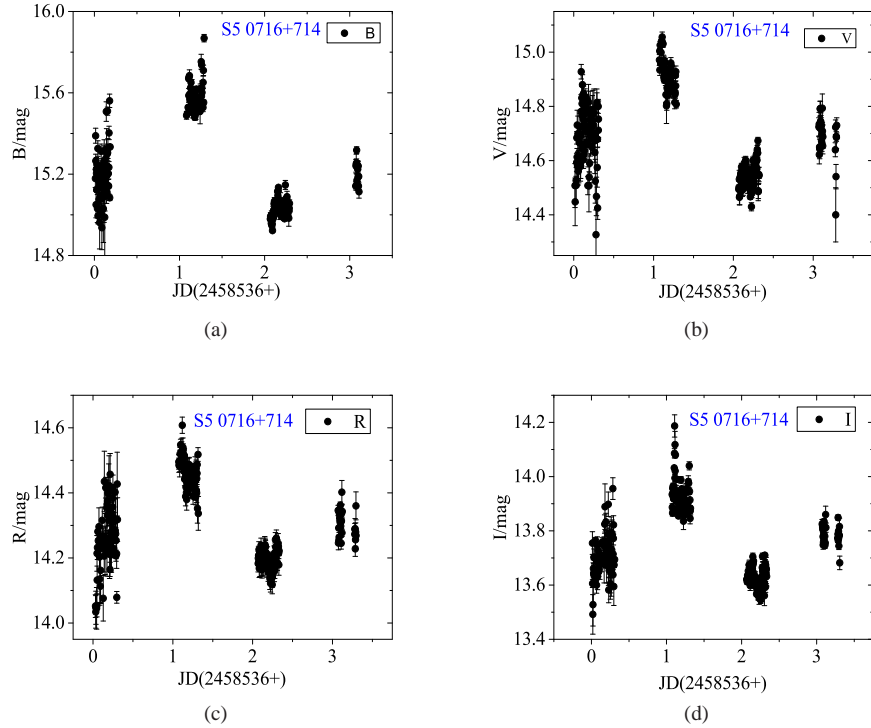
The B , V , R , I ($BVRI$) band light curves of S5 0716+714 are shown in Figure 1, and they are listed in Table 1, in which Col. (1), Band; Col. (2), JD-2458536; Col. (3), brightness, in units of mag; Col. (4), the standard deviation of Col. (3), in units of mag.

For S5 0716+714, there are 990 observations, among them, the maximum variance are respectively, $\Delta m_B = 0.237 \pm 0.008$ mag, $\Delta m_V = 0.432 \pm 0.051$ mag, $\Delta m_R = 0.202 \pm 0.006$ mag, $\Delta m_I = 0.321 \pm 0.029$ mag.

2. 3C 273

The B , V , R , I ($BVRI$) band light curves of 3C 273 are shown in Figure 2, and they are listed in Table 2, in which Col. (1), Band; Col. (2), JD-2458536; Col. (3), brightness, in units of mag; Col. (4), the standard deviation of Col. (3), in units of mag.

For 3C 273, there are 884 observations, among which, the maximum variances are respectively, $\Delta m_B = 0.075 \pm 0.018$ mag, $\Delta m_V = 0.035 \pm 0.015$ mag, $\Delta m_R = 0.076 \pm 0.02$ mag, $\Delta m_I = 0.055 \pm 0.018$ mag.

**Fig. 1** The *BVRI* light curves of S5 0716+714.**Table 1** The *BVRI* Observations of S5 0716+714

Band	JD	<i>m</i> (mag)	σ (mag)												
(1)	(2)	(3)	(4)	(1)	(2)	(3)	(4)	(1)	(2)	(3)	(4)	(1)	(2)	(3)	(4)
<i>B</i>	0.011	15.179	0.044	<i>V</i>	0.015	14.593	0.081	<i>R</i>	0.174	14.281	0.070	<i>I</i>	0.013	13.755	0.042
<i>B</i>	0.014	15.389	0.037	<i>V</i>	0.017	14.533	0.088	<i>R</i>	0.207	14.232	0.094	<i>I</i>	0.016	13.606	0.015
<i>B</i>	0.016	15.265	0.033	<i>V</i>	0.028	14.612	0.015	<i>R</i>	0.081	14.270	0.037	<i>I</i>	0.018	13.492	0.073
<i>B</i>	0.019	15.050	0.065	<i>V</i>	0.030	14.594	0.065	<i>R</i>	0.034	14.101	0.050	<i>I</i>	0.021	13.528	0.079
<i>B</i>	0.022	15.224	0.039	<i>V</i>	0.036	14.678	0.034	<i>R</i>	0.091	14.180	0.050	<i>I</i>	0.024	13.606	0.076
<i>B</i>	0.024	15.204	0.078	<i>V</i>	0.038	14.769	0.023	<i>R</i>	0.227	14.282	0.055	<i>I</i>	0.026	13.661	0.032
<i>B</i>	0.027	15.123	0.008	<i>V</i>	0.041	14.698	0.032	<i>R</i>	0.182	14.442	0.038	<i>I</i>	0.029	13.644	0.036
...
...
...

This full table is available in <http://www.raa-journal.org/docs/Supp/ms4773table1.pdf>.

3.1 Intra-day Optical Variability

3.1.1 Method

We use the variability amplitude (Amp), F-test and C-test method to analyze the intra-day variability.

1. Amp

Variability amplitude (Amp) (Heidt & Wagner 1996) can be used to measure the variability of every day, which can be introduced as the following,

$$A = 100 \times \sqrt{((m_{\max} - m_{\min})^2 - 2\sigma^2)\%}, \quad (1)$$

where m_{\max} and m_{\min} are the maximum and minimum magnitude, σ is the RMS error.

2. C-test

The C-test is calculated as (Romero et al. 1999):

$$C_1 = \frac{\sigma(m_S - m_{\text{Com1}})}{\sigma(m_{\text{Com1}} - m_{\text{Com2}})}, \quad (2)$$

$$C_2 = \frac{\sigma(m_S - m_{\text{Com2}})}{\sigma(m_{\text{Com1}} - m_{\text{Com2}})},$$

where $\sigma(m_S - m_{\text{Com1}})$, $\sigma(m_S - m_{\text{Com2}})$, and $\sigma(m_{\text{Com1}} - m_{\text{Com2}})$ are the standard deviations of the differences of instrumental magnitudes between the source and comparison ‘1’, the differences between the source and comparison ‘2’, and the differences between two comparisons ‘1’ and ‘2’, respectively. If the variability criterion requires $C \geq 2.576$, the variable corresponds to a 99 percent confidence level.

3. F-test

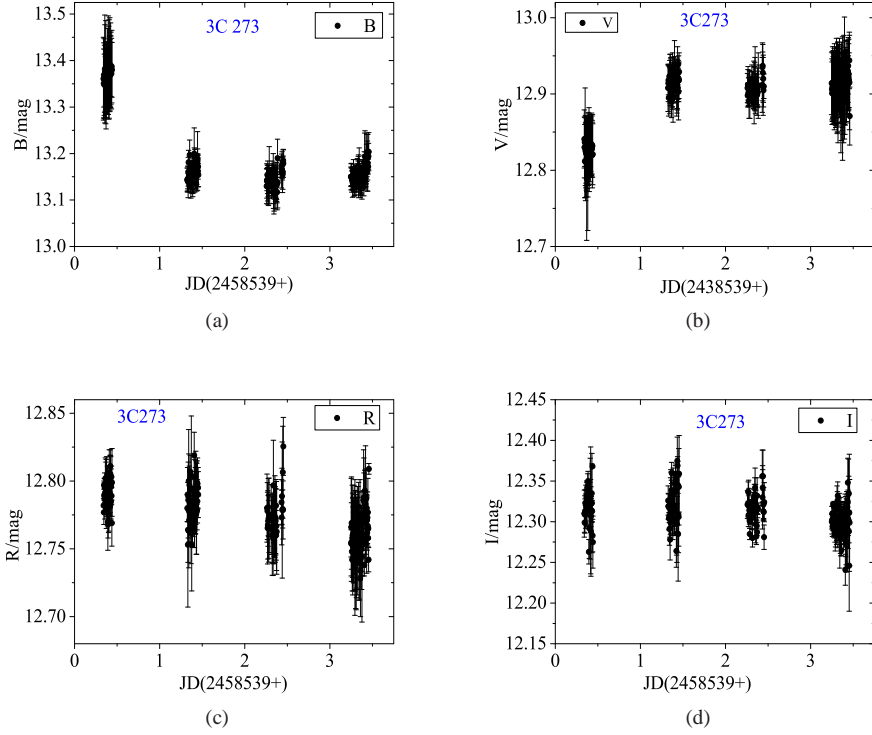


Fig. 2 The *BVRI* light curves of 3C 273.

Table 2 The *BVRI* Observations of 3C 273

Band	JD	m (mag)	σ (mag)												
(1)	(2)	(3)	(4)	(1)	(2)	(3)	(4)	(1)	(2)	(3)	(4)	(1)	(2)	(3)	(4)
<i>B</i>	0.340	13.361	0.089	<i>V</i>	0.340	12.841	0.038	<i>R</i>	0.341	12.782	0.005	<i>I</i>	0.342	12.310	0.029
<i>B</i>	0.342	13.351	0.074	<i>V</i>	0.343	12.830	0.040	<i>R</i>	0.343	12.777	0.009	<i>I</i>	0.344	12.299	0.012
<i>B</i>	0.345	13.369	0.069	<i>V</i>	0.345	12.837	0.032	<i>R</i>	0.346	12.797	0.003	<i>I</i>	0.347	12.309	0.023
<i>B</i>	0.347	13.361	0.086	<i>V</i>	0.348	12.812	0.048	<i>R</i>	0.349	12.789	0.013	<i>I</i>	0.349	12.313	0.015
<i>B</i>	0.350	13.348	0.066	<i>V</i>	0.350	12.836	0.072	<i>R</i>	0.351	12.790	0.009	<i>I</i>	0.352	12.323	0.016
<i>B</i>	0.352	13.361	0.072	<i>V</i>	0.353	12.826	0.046	<i>R</i>	0.354	12.795	0.011	<i>I</i>	0.354	12.309	0.011
...
...
...

This full table is available in <http://www.raa-journal.org/docs/Supp/ms4773table2.pdf>.

F values are very reliable (de Diego 2010), and can be introduced as:

$$F_1 = \frac{\text{Var}(m_S - m_1)}{\text{Var}(m_1 - m_2)}, F_2 = \frac{\text{Var}(m_S - m_2)}{\text{Var}(m_1 - m_2)}, \quad (3)$$

where $\text{Var}(m_S - m_1)$, $\text{Var}(m_S - m_2)$, $\text{Var}(m_1 - m_2)$ are the variances of instrumental magnitudes difference.

F_{v_{bl}, v_*}^α is the critical F -value, v_{bl} and v_* are the number of degrees of freedom for the blazar and the comparison star respectively, and χ is the significance level set as 0.01(2.6σ). If the average F value (the average of F_1 and F_2) is larger than the critical value, the blazar is variable at the confidence level of 99%.

4. Multi-bands mutual verification

On every day, our observations cover four bands (*B*, *V*, *R*, *I*), so we can use the following method to make

mutual verification.

- (1) If there lies intra-day variability only at one band, which should be unreliable.
- (2) If there lie intra-day variabilities at two bands, which should be uncertain.
- (3) If there lie intra-day variabilities at more than two bands, which should be reliable.

3.1.2 Result

When a light curve obeys the requirements: (1) the optical variability (Δm) is more than three times sigma (σ) (Fan et al. 2009b; Fan et al. 2014); (2) the variability parameter $C \geq 2.576$ (Romero et al. 1999); (3) the F -test value is higher than the critical value (Fan et al. 2018; de Diego 2010); (4) if there are more than two bands lying

variabilities, we think intra-day variability (IDV) occurred. In the calculation, we use Δm to represent the biggest brightness variability, with σ being the corresponding standard deviation, and Δt being the time span of Δm .

Our results about the IDVs are listed in Tables 3 and 4, in which,

- Col. (1) observation date;
- Col. (2) band;
- Col. (3) number of observations;
- Col. (4) C-test value;
- Col. (5) F-test value;
- Col. (6) the critical value of F-test (at the 99% confidence level);
- Col. (7) variability amplitude;
- Col. (8) Δt , time span (the timescale of optical variability), in units of hour;
- Col. (9) $\Delta m \pm \sigma$, variable value (the difference between maximum and minimum of peak) and the corresponding standard deviation, in unit of mag;
- Col. (10) the state of optical variability (V: variability, U: uncertain, N: non-variability).

(1) S5 0716+714

From Table 3, we can see that, for S5 0716+714, there are IDVs on three nights, Feb.23, Feb.24, Feb.25, whose intra-day light curves have been shown in Figure 3, where, the black dots stand for intra-day light curves, and the red dots stand for the magnitude differences between two comparison stars ‘5’ and ‘6’.

On JD 2458539, at R band, the source brightens by $\Delta m_R = 0.119$ mag within 100.8 minutes from JD 2458539.155 to JD 2458539.225. The brightness can fade by $\Delta m_R = 0.139$ mag within 100.8 minutes from JD 2458539.25 to JD 2458539.297, with the variable amplitudes 92.4%. At I band, the brightness can fade by 0.091 mag within 62.8 min and brighten by 0.096 mag within 129 min.

(2) 3C 273

From Table 4, we can see that, for 3C 273, on Feb.25 and Feb.26, there lie variabilities at two bands (R and I), so those variabilities are uncertain, see Figure 4, where the black dots stand for the light curves and the red dots stand for the magnitude difference between comparison stars ‘C’ and ‘D’.

There may lie IDVs, with the variable values $\Delta m_R = 0.076 \pm 0.02$ mag within 30 min at R band, and $\Delta m_I = 0.082 \pm 0.012$ mag within 25.8 min at I band.

3.2 Optical Spectral Indices

3.2.1 Procedure

According to Fan et al. (2014), Yuan et al. (2017) and Xiong et al. (2017), and so on, we obtain the following method to calculate the optical spectral index.

First, we make the Galactic extinction correction from NED (<http://ned.ipac.caltech.edu/>). For S5 0716+714, $A_B = 0.112$ mag, $A_V = 0.085$ mag, $A_R = 0.067$ mag, $A_I = 0.047$ mag; and for 3C 273, $A_B = 0.075$ mag, $A_V = 0.057$ mag, $A_R = 0.045$ mag, $A_I = 0.031$ mag. Second, we convert the magnitude (m_ν) into flux density (F_ν), then use the relation $F_\nu \propto \nu^{-\alpha}$ to calculate the spectral index (α), here, the frequency is $\nu_B = 6.81 \times 10^{14}$ Hz, $\nu_V = 5.45 \times 10^{14}$ Hz, $\nu_R = 4.68 \times 10^{14}$ Hz, $\nu_I = 3.75 \times 10^{14}$ Hz (Here ν is frequency). Lastly, based on the relation $\log(F_\nu) = -\alpha \log(\nu) + \text{const}$, we obtain spectral indices (α).

Subsequently, we use the linear fitting to analyze the relations between α and $F_\nu (\nu = V, R, I)$: $F_\nu = k \times \alpha + b$. In this process, r is the Pearson’s correlation coefficient, which can be expressed as:

$$r = \frac{\sum(x_i - \bar{x})(y_j - \bar{y})}{\sqrt{\sum(x_i - \bar{x})^2} \sqrt{\sum(y_j - \bar{y})^2}}, \quad (4)$$

where x_i is $F_{V,R,I}$, y_i is α , \bar{x} is the average value of α , and \bar{y} is the average value of $F_\nu (\nu = V, R, I)$, p is the chance probability of linear fitting.

3.2.2 Result

(1) S5 0716+714

For S5 0716+714, we obtain 218 spectral indices (α), which are in the range from 0.432 ± 0.027 to 2.146 ± 0.156 , with the average value $\bar{\alpha} = 1.41 \pm 0.22$.

The correlations between $F_\nu (\nu = B, V, R, I)$ and α are shown in Figure 5, where the black dots stand for the distributions between F_ν and α , the red lines stand for the linear fitting.

For the whole sample, the linear correlations between F_ν and α are as the following:

at V band, $\alpha = (-0.148 \pm 0.016)F_V + (2.153 \pm 0.08)$, with $r_V = -0.531$ and $p < 0.0001$, which imply a strong anti-correlation;

at R band, $\alpha = (-0.045 \pm 0.022)F_R + (1.679 \pm 0.13)$, with $r_R = -0.139$ and $p = 3.99 \times 10^{-2}$, which imply weak anti-correlation;

at I band, $\alpha = (-1.73 \pm 1.48) \times 10^{-2} F_I + (1.267 \pm 0.123)$, with $r_I = -0.009$ and $p = 0.898$, which imply no correlation.

(2) 3C 273

For 3C 273, we obtain 216 spectral indices (α), which are in range from -0.148 ± 0.001 to -0.086 ± 0.001 , with the average value $\bar{\alpha} = -0.127 \pm 0.009$.

For the whole sample, the linear correlations between F_ν and α are as the following:

at V band, $\alpha = (-0.205 \pm 0.011)F_V + (2.518 \pm 0.139)$, with $r_V = -0.792$ and $p < 0.0001$, which show a strong anti-correlation;

at R band, $\alpha = (0.167 \pm 0.029)F_R - (2.266 \pm 0.36)$, with

Table 3 The IDV Results of S5 0716+714

Date (1)	Band (2)	<i>N</i> (3)	<i>C</i> (4)	<i>F</i> (5)	$F_C(99)$ (6)	<i>A</i> (%) (7)	Δt (h) (8)	$\Delta m \pm \sigma$ (mag) (9)	<i>V/N/U</i> (10)
2019 Feb 21	<i>B</i>	65	1.719	2.956	1.8	0.777	-	-	<i>N</i>
2019 Feb 21	<i>V</i>	106	6.026	6.097	1.579	0.888	2.2	0.432 ± 0.051	<i>N</i>
2019 Feb 21	<i>R</i>	96	2.003	4.04	1.618	0.938	-	-	<i>N</i>
2019 Feb 21	<i>I</i>	92	1.118	1.31	1.635	0.501	-	-	<i>N</i>
2019 Feb 23	<i>B</i>	72	10.783	116.977	1.747	0.438	2.64	0.396 ± 0.001	<i>V</i>
2019 Feb 23	<i>V</i>	72	4.665	21.776	1.747	0.309	1.38	0.246 ± 0.006	<i>V</i>
2019 Feb 23	<i>R</i>	90	13.439	180.753	1.644	0.268	1.49	0.202 ± 0.006	<i>V</i>
2019 Feb 23	<i>I</i>	94	14.984	225.462	1.626	0.434	0.69	0.321 ± 0.029	<i>V</i>
2019 Feb 24	<i>B</i>	69	3.94	16.06	1.768	0.224	1.67	0.212 ± 0.001	<i>V</i>
2019 Feb 24	<i>V</i>	88	6.437	42.245	1.653	0.236	2.3	0.206 ± 0.003	<i>V</i>
2019 Feb 24	<i>R</i>	91	7.024	49.385	1.639	0.071	1.75	0.139 ± 0.003	<i>V</i>
2019 Feb 24	<i>I</i>	89	4.932	24.328	1.649	0.178	2.5	0.16 ± 0.0001	<i>V</i>
2019 Feb 25	<i>B</i>	16	4.971	4.971	3.522	0.321	0.33	0.129 ± 0.008	<i>V</i>
2019 Feb 25	<i>V</i>	27	4.535	46.383	3.027	0.202	0.25	0.169 ± 0.007	<i>V</i>
2019 Feb 25	<i>R</i> (1)	20	8.519	82.832	3.027	0.157	0.56	0.116 ± 0.011	<i>V</i>
2019 Feb 25	<i>R</i> (2)	8	8.498	62.931	6.993	0.127	0.19	0.132 ± 0.02	<i>V</i>
2019 Feb 25	<i>I</i>	31	13.7	105.725	4.849	0.233	0.31	0.086 ± 0.005	<i>V</i>

Table 4 The IDV Results of 3C 273

Date (1)	Band (2)	<i>N</i> (3)	<i>C</i> (4)	<i>F</i> (5)	$F_C(99)$ (6)	<i>A</i> (%) (7)	Δt (h) (8)	$\Delta m \pm \sigma$ (mag) (9)	<i>V/N/U</i> (10)
2019 Feb 24	<i>B</i>	40	1.357	1.85	2.135	0.04	-	-	<i>N</i>
2019 Feb 24	<i>V</i>	40	1.842	3.416	2.135	0.032	-	-	<i>N</i>
2019 Feb 24	<i>R</i>	40	2.344	5.52	2.135	0.041	-	-	<i>N</i>
2019 Feb 24	<i>I</i>	39	8.612	74.675	2.157	0.101	0.78	0.072 ± 0.02	<i>N</i>
2019 Feb 25	<i>B</i>	53	1.789	3.222	1.923	0.084	-	-	<i>N</i>
2019 Feb 25	<i>V</i>	51	1.962	4.135	1.949	0.089	-	-	<i>N</i>
2019 Feb 25	<i>R</i>	52	4.478	21.38	1.936	0.119	0.49	0.076 ± 0.02	<i>U</i>
2019 Feb 25	<i>I</i>	50	5.927	35.429	1.963	0.277	0.43	0.082 ± 0.012	<i>U</i>
2019 Feb 26	<i>B</i>	54	1.647	2.761	1.911	0.071	-	-	<i>N</i>
2019 Feb 26	<i>V</i>	55	2.461	6.13	1.899	0.183	-	-	<i>N</i>
2019 Feb 26	<i>R</i>	53	5.426	30.387	1.923	0.26	0.36	0.068 ± 0.025	<i>U</i>
2019 Feb 26	<i>I</i>	53	4.39	19.4	1.923	0.484	0.55	0.055 ± 0.02	<i>U</i>
2019 Feb 27	<i>B</i>	83	1.173	1.387	1.679	0.071	-	-	<i>N</i>
2019 Feb 27	<i>V</i>	83	2.132	4.644	1.679	0.071	-	-	<i>N</i>
2019 Feb 27	<i>R</i>	82	2.135	5.416	1.684	0.153	-	-	<i>N</i>
2019 Feb 27	<i>I</i>	81	3.11	9.724	1.69	0.104	0.94	0.042 ± 0.02	<i>N</i>

$r_R = 0.372$ and $p < 0.0001$, which show weak correlation; at *I* band, $\alpha = (0.253 \pm 0.02) F_I - (3.24 \pm 0.223)$, with $r_I = 0.69$ and $p < 0.0001$, which show strong positive correlation.

3.3 Time Delays Among Different Bands

To analyze the time delays among different bands, we use the discrete correlation function (DCF) method to deal with the uneven data. This method was introduced by Edelson & Krolik (1988), and can be used to analyze the time delays from time series of different bands. We get time lags by exploring the correlations from two variable temporal sets with DCF method. To get the result, first, we calculate the unbinned correlation (UDCF) of two data stream, which can be defined as:

$$\text{UDCF}_{ij} = \frac{(x_i - \bar{x}) \times (y_j - \bar{y})}{\sqrt{\sigma_x \times \sigma_y}}, \quad (5)$$

where x_i, y_j are two data streams, \bar{x} and \bar{y} are the average values of the data sets, σ_x and σ_y are the corresponding standard deviations.

Second, we average the UDCF points according to each lag τ , and obtain $\text{DCF}(\tau)$,

$$\text{DCF}(\tau) = \frac{1}{N} \sum \text{UDCF}_{ij}(\tau), \quad (6)$$

where N is the total number of data pairs (x_i, y_j) . The standard error of each bin is

$$\sigma(\tau) = \frac{1}{N} (\sum [\text{UDCF}_{ij} - \text{DCF}(\tau)]^2)^{0.5}. \quad (7)$$

Finally, we use the Gaussian function to fit the DCF results, and obtain the delay time.

For S5 0716+714, the calculated results are shown in Figure 6. On JD 2458538, the time delay is $\tau_{RB} = 12.72 \pm 8.35$ min between *R* and *B* bands. On JD 2458539, the

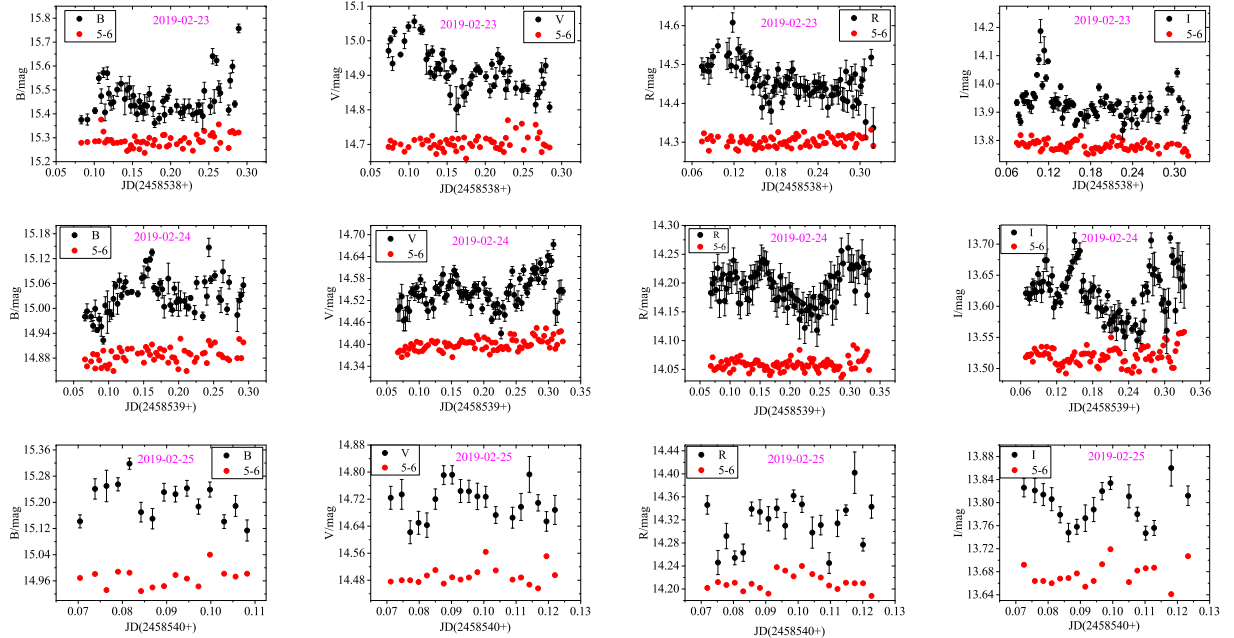


Fig. 3 The IDV light curves of S5 0716+714 at *BVRI* bands. From top to bottom, every row stand for the light curves on Feb.23, Feb.24 and Feb.25 respectively, where, the black dots stand for the optical variability and the red dots stand for the magnitude difference between comparison stars ‘5’ and ‘6’.

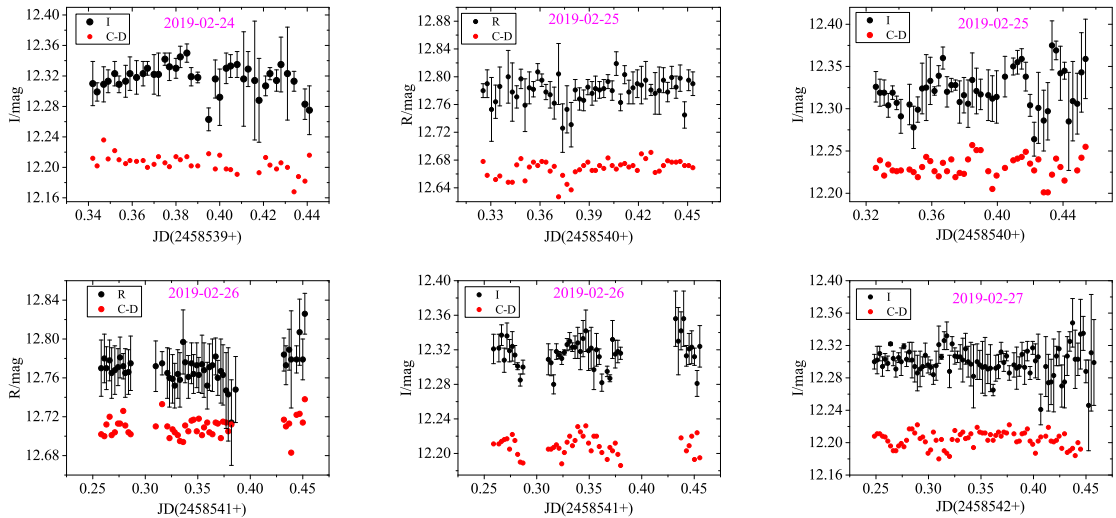


Fig. 4 The IDV light curves of 3C 273 at *RI* bands. The black dots stand for the light curves and the red dots stand for the magnitude difference between comparison stars ‘C’ and ‘D’.

time delay is $\tau_{RV} = 18.58 \pm 1.73$ min between *R* and *V* bands, $\tau_{RI} = 3.46 \pm 1.44$ min between *R* and *I* bands.

For 3C 273, the calculated results are shown in Figure 7. On JD 2458540, the time delay is $\tau_{IB} = 16.76 \pm 5.47$ min between *I* and *B* bands, $\tau_{IR} = 11.19 \pm 2.72$ min between *I* and *R* bands. On JD 2458541, the time delay is $\tau_{IR} = 22.176 \pm 3.3$ min between *I* and *R* bands. On JD 2458542, the time delay is $\tau_{IB} = 9.48 \pm 3.15$ min

between *I* and *B* bands, $\tau_{IV} = 6.42 \pm 3.37$ min between *I* and *V* bands.

3.4 Intra-day Periodicity

3.4.1 Method

Generally, the intra-day light curves of blazars show uneven distributions, and thus we chose the power

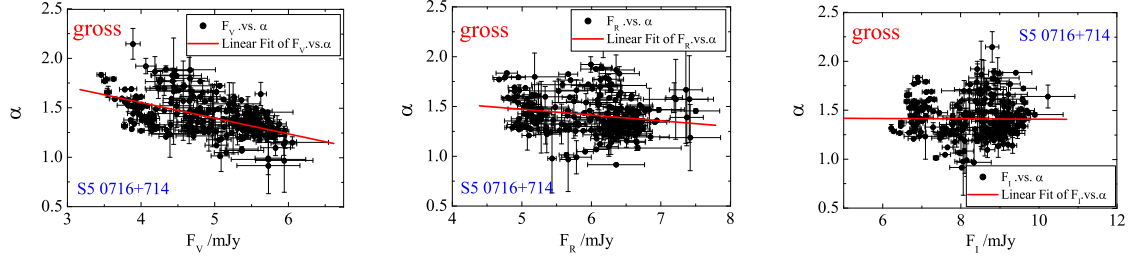


Fig. 5 The correlations between α and F_{VRI} of S5 0716+714 based on the total sample, with the red lines stand for the linear fitting.

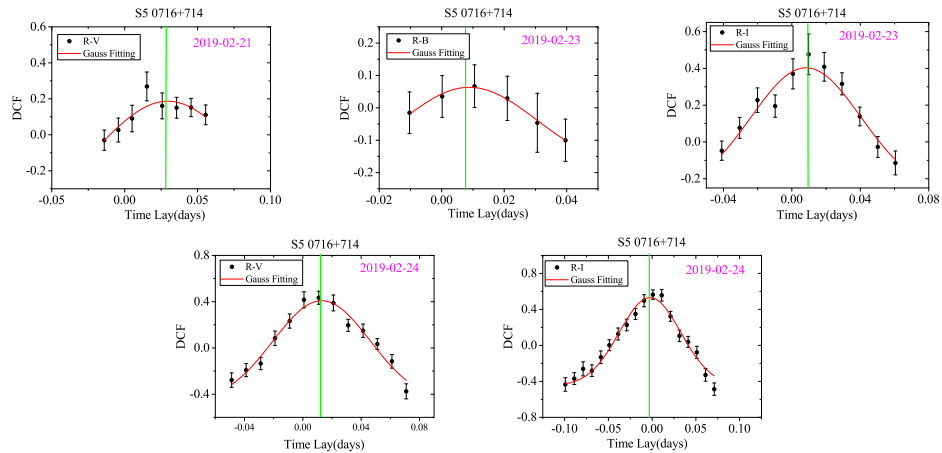


Fig. 6 The time delays among different bands of S5 0716+714. The black dots with errorbar stand for the DCF results, and the red lines stand for Gaussian fitting.

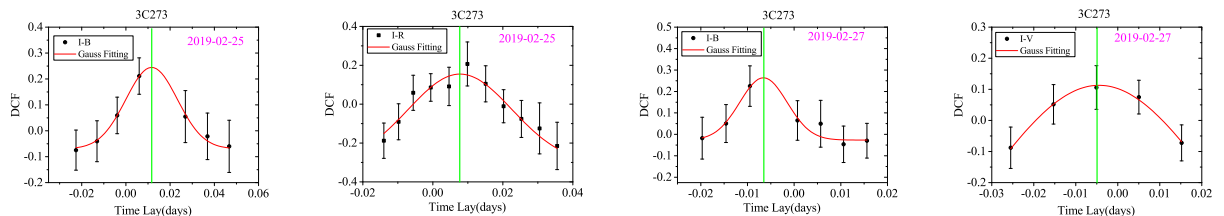


Fig. 7 The time delays among different bands of 3C 273. The black dots with errorbar stand for the DCF results, and the red lines stand for Gaussian fitting.

spectrum (PS) and DCF method (Fan & Lin 2000) to deal with this question.

Power Spectrum Analysis: The most commonly used tool for periodicity analysis of both evenly and unevenly sampled signals is the Periodogram method, which is an estimator of the signal energy in the frequency domain (Deeming 1975). Lomb (1976) introduced a modified form of this method, which can be described as follows. Considering a series $x(n)$ with N points, then let f be the frequency and τ be a variable timescale. Their mean and deviation are given by: $\bar{x} = \frac{1}{N} \sum_{n=1}^N x(n)$ and $\sigma^2 = \frac{1}{N} \sum_{n=1}^N (x(n) - \bar{x})^2$. The normalized Lomb's P^L , i.e.

the power spectrum as a function of the angular frequency $\omega \equiv 2\pi f > 0$ is defined as:

$$P_N^L(\omega) = \frac{1}{2\sigma^2} \left[\frac{\sum_{n=0}^{N-1} (x(n) - \bar{x}) \cos \omega(t_n - \tau)]^2}{\sum_{n=0}^{N-1} \cos^2 \omega(t_n - \tau)} \right] + \frac{1}{2\sigma^2} \left[\frac{\sum_{n=0}^{N-1} (x(n) - \bar{x}) \sin \omega(t_n - \tau)]^2}{\sum_{n=0}^{N-1} \sin^2 \omega(t_n - \tau)} \right], \quad (8)$$

and τ is defined by the equation:

$$\tan(2\omega\tau) = \frac{\sum_{n=0}^{N-1} \sin 2\omega t_n}{\sum_{n=0}^{N-1} \cos 2\omega t_n}. \quad (9)$$

We calculate the error of the period by calculating the full width at half maximum (FWHM) of the periodic signals, and use the red noise (Schulz & Mudelsee 2002) to measure the PS results.

3.4.2 Result

For S5 0716+714, based on DCF and PS method, it is possible that there lie periods at B and I bands on JD 2458539, which have been shown in Figure 8 and Figure 9. In Figure 8, the dot lines stand for the DCF result, and the red lines stand for Gaussian fitting. In Figure 9, the black lines stand for the PS results; the red, green, blue, cyan lines stand for the 80%, 90%, 95% and 99% red noise levels, respectively; the red dashed lines stand for Gaussian fitting.

The main results have been listed in Table 5, where, Col. (1): Name;
 Col. (2): JD;
 Col. (3): Method;
 Col. (4): P_B , period at B band, in units of min;
 Col. (5): P_V , period at V band, in units of min;
 Col. (6): P_R , period at R band, in units of min;
 Col. (7): P_I , period at I band, in units of min;
 Col. (8): \bar{P} , the averaged period different bands, in units of min.

From Table 5, we can see that for S5 0716+714, the DCF results might be two times of the PS results. Considering the DCF results, the averaged period of two bands is $\bar{P} = 185.78 \pm 81.17$ min. On every day, our observations cover ~ 6 hours, which is only two times of \bar{P} , so it is necessary to verify the period with more data.

For 3C 273, based on DCF and PS method, we find intra-day periods on JD 2458540, JD 2458541 and JD 2458542, see Figures 10 and 11.

The main results have been listed in Table 5. On JD2458540 and JD2458541, the periods are consistent with each other, which is about 60 min. On JD 2458542, the period is about 80 min.

4 DISCUSSION AND CONCLUSIONS

4.1 Optical Variabilities

During our monitored duration, we obtain the following observations. For S5 0716+714, there are 990 observations. At B band, there are 197 observations, which cover from 14.93 ± 0.01 mag to 15.76 ± 0.02 mag, with the averaged value $\bar{m}_B = 15.22 \pm 0.19$ mag. At V band, there are 250 observations, which cover from 14.4 ± 0.1 mag to 15.06 ± 0.02 mag, with the averaged value $\bar{m}_V = 14.72 \pm 0.17$ mag. At R band, there are 272 observations, which cover from 14.101 ± 0.05 mag to 14.608 ± 0.025 mag, with the averaged value $\bar{m}_R = 14.32 \pm 0.12$ mag. At I band, there are 271 observations, which cover from 13.492 ± 0.07 mag

to 14.187 ± 0.04 mag, with the averaged value $\bar{m}_I = 13.75 \pm 0.14$ mag. The IDV timescales of S5 0716+714 are in the range from 0.31 hours ($\Delta m = 0.086 \pm 0.005$ mag) to 2.64 hours ($\Delta m = 0.396 \pm 0.001$ mag).

Yuan et al. (2017) used the observations from 2000 to 2014 and found that the variable ranges at VRI bands were $12.44 \pm 0.02 \sim 15.11 \pm 0.01$ mag at V band, $11.67 \pm 0.04 \sim 14.59 \pm 0.08$ mag at R band and $11.31 \pm 0.03 \sim 14.09 \pm 0.02$ mag at I band respectively, which are consistent with our results.

For 3C 273, there are 884 observations. At B band, there are 225 observations, which cover from 13.12 ± 0.05 mag to 13.39 ± 0.1 mag, with the averaged value $\bar{m}_B = 13.19 \pm 0.09$ mag. At V band, there are 219 observations, which cover from 12.79 ± 0.08 mag to 12.94 ± 0.04 mag, with the averaged value $\bar{m}_V = 12.9 \pm 0.04$ mag. At R band, there are 224 observations, which cover from 12.69 ± 0.05 mag to 12.85 ± 0.02 mag, with the averaged value $\bar{m}_R = 12.77 \pm 0.02$ mag. At I band, there are 216 observations, which cover from 12.24 ± 0.02 mag to 12.5 ± 0.04 mag, with the averaged value $\bar{m}_I = 12.31 \pm 0.03$ mag, and brighten by $\Delta R = 0^m.08$ in 22 minutes. The IDV timescales are 0.36 hours ($\Delta m = 0.068 \pm 0.025$ mag) and 0.49 hours ($\Delta m = 0.076 \pm 0.02$ mag).

Based on the observations in 2000 to 2014, Fan et al. (2014) obtained that the magnitude distributions at V , R and I bands were $12.9 \sim 12.5$ mag, $12.8 \sim 12.3$ mag and $12.2 \sim 11.85$ mag, respectively. Xiong et al. (2017) analyzed the observations of 3C 273 from 2005–2016 and obtained that the variable ranges at VRI bands were, $13.1 \sim 12.42$ mag at V band, $13.09 \sim 12.37$ mag at R band and $12.59 \sim 11.93$ mag at I band, respectively. Based on the upper comparisons, we can find that our results are consistent with the others.

4.2 Doppler Factor

A relativistic jet is the typical characteristic of blazars. The fluxes of blazars can be strongly increased by a factor of $\delta^{2+\alpha}$ considering a stationary jet, or by a factor of $\delta^{3+\alpha}$ considering of distinct ‘blobs’ in the jet (Blandford & Königl 1979). So the Doppler factor (δ) is very important in studying the origins of the physical processes in the compact emission region of Blazars, which have been studied by many papers (Ghisellini et al. 1993; Hartman et al. 1999; Fan et al. 2009a; Savolainen et al. 2010; Fan et al. 2014; Yuan et al. 2017).

We use the method from Fan et al. (2013) to calculate the lower limit of the Doppler factor (δ),

$$\delta \geq [1.54 \times 10^{-3} (1+z)^{4+2\alpha} (\frac{d_L}{\text{Mpc}})^2 (\frac{\Delta T}{\text{h}})^{-1} \times (\frac{F_{\text{keV}}}{\mu\text{Jy}}) (\frac{E_\gamma}{\text{GeV}})^\alpha]^{1/(4+2\alpha)}, \quad (10)$$

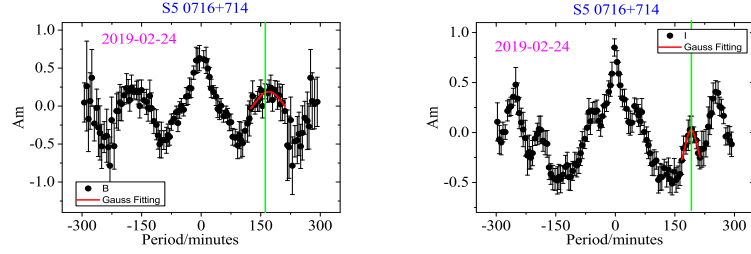


Fig. 8 Intra-day period of S5 0716+714 calculated by the DCF method, where the *black dots* stand for DCF results and the *red lines* stand for the Gaussian fitting.

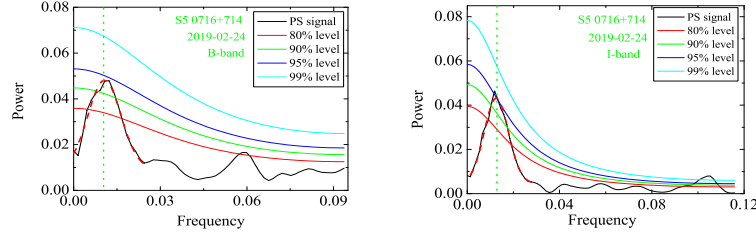


Fig. 9 Intra-day period of S5 0716+714 calculated by the PS method, where the *black lines* stand for the PS signal, the *red, green, blue* and *cyan lines* stand for the 80%, 90%, 95% and 99% red noise levels, respectively.

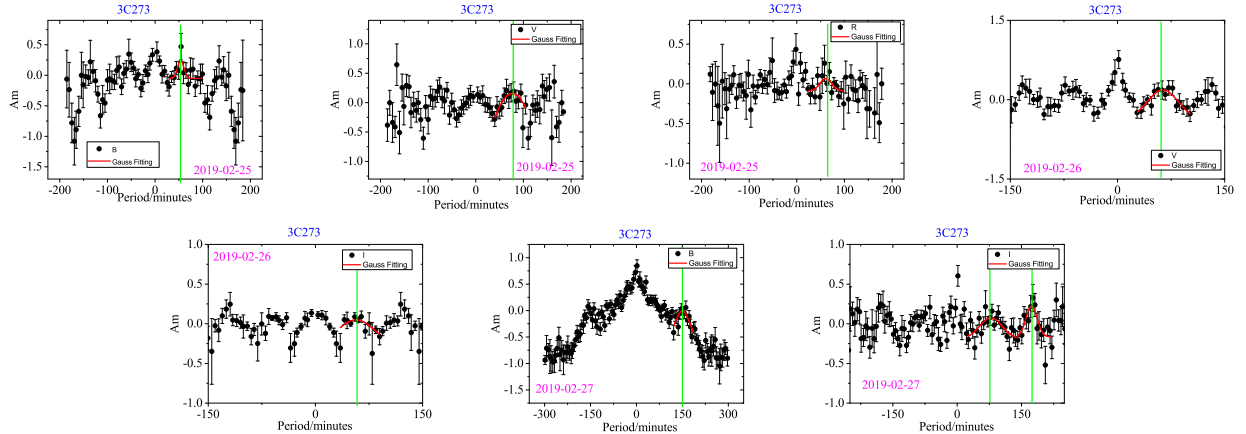


Fig. 10 Intra-day periods of 3C 273 calculated by DCF methods, where the *black dots* stand for DCF results and the *red lines* stand for the Gaussian fitting.

Table 5 Intra-day Periods of S5 0716+714 and 3C 273

Source	JD	Method	P_B (min) (4)	P_V (min) (5)	P_R (min) (6)	P_I (min) (7)	\bar{P} (min) (8)
(1)	(2)	(3)	(4)	(5)	(6)	(7)	(8)
S5 0716+714	2458539	DCF PS	170.36 ± 45.19	-	-	191.05 ± 22.32 79.93 ± 26.74	185.78 ± 81.17 92.58 ± 63.59
3C 273	2458540	DCF PS	53.80 ± 13.96 62.03 ± 19.93	76.78 ± 23.08 52.80 ± 16.07	61.16 ± 16.08 87.18 ± 38.43	-	63.91 ± 31.40 67.33 ± 46.18
	2458541	DCF PS	-	63.33 ± 17.54 67.52 ± 26.79	-	56.85 ± 17.15 51.55 ± 13.52	60.09 ± 24.53 59.54 ± 30.00
	2458542	DCF PS	-	-	-	78.63 ± 20.18 81.37 ± 24.87	78.63 ± 20.18 81.37 ± 24.87

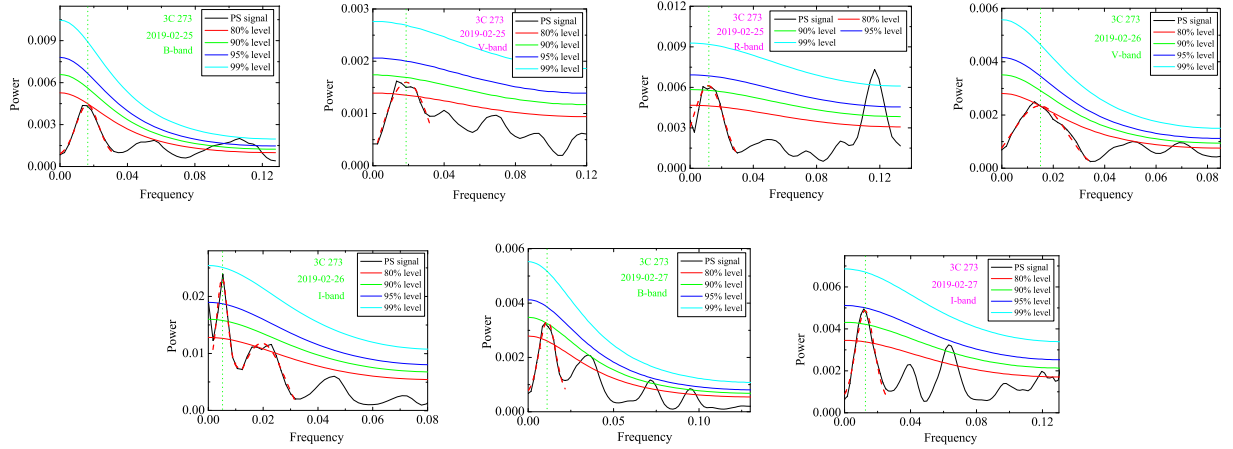


Fig. 11 Intra-day periods of 3C 273 calculated by PS methods, where the *black lines* stand for the PS signal, the *red, green, blue and cyan lines* stand for the 80%, 90%, 95% and 99% red noise level, respectively.

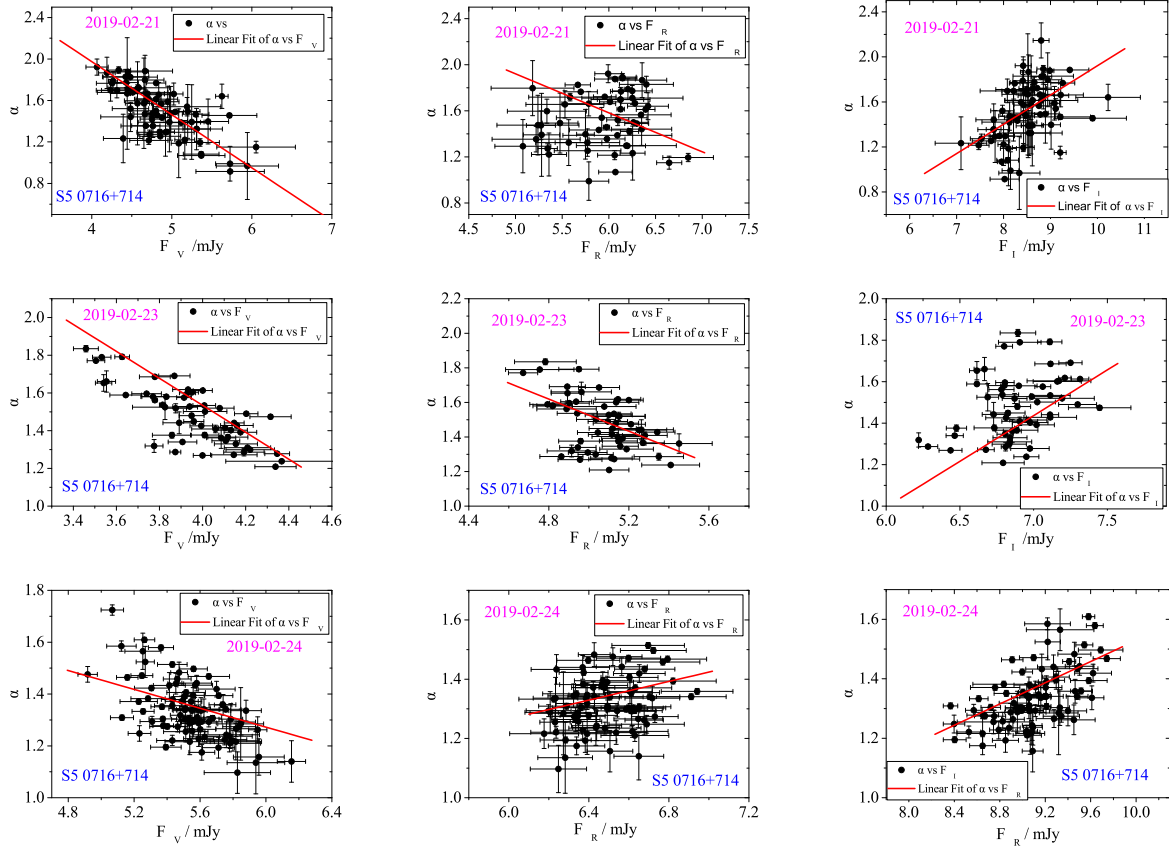


Fig. 12 The correlations between α and F_{VRI} of S5 0716+714 on every day. The upper row stands for the results on JD 2458536, the middle row stands for the results on JD 2458538, the lower row stands for the results on JD 2458539, while the *red lines* stand for the linear fittings.

where α is the X-ray spectral index ($F_X \propto \nu_X^{-\alpha}$), F_{keV} is the flux density at 1 keV, E_γ is the γ -ray energy, d_L is the luminosity distance and ΔT is IDV timescales, in units of hours.

For S5 0716+714, our minimum timescales ΔT is 0.058h, $d_L = 1499$ Mpc (NED), $F_{\text{keV}} = 0.99\mu\text{Jy}$, $\alpha=1.77$ (Donato et al. 2001), $E_\gamma=4.59$ GeV (Fan et al. 2014), so we obtain $\delta \geq 8.096$. For a comparison, from the literature,

Table 6 Linear Correlations of S5 0716+714 between F_ν and α

JD	F_ν .vs. α	$k \pm \Delta k$	$b \pm \Delta b$	r	p
2458536	α .vs. F_V	$-0.512 \pm 3.09 \times 10^{-5}$	$4.028 \pm 1.49 \times 10^{-4}$	-0.813	< 0.0001
	α .vs. F_R	$-0.339 \pm 3.68 \times 10^{-5}$	$3.614 \pm 2.24 \times 10^{-4}$	-0.452	4.15×10^{-4}
	α .vs. F_I	$0.259 \pm 2.07 \times 10^{-5}$	$-0.676 \pm 2.29 \times 10^{-4}$	0.478	< 0.0001
2458538	α .vs. F_V	$-0.715 \pm 8.58 \times 10^{-12}$	$4.39 \pm 3.5 \times 10^{-11}$	-0.813	< 0.0001
	α .vs. F_R	$-0.46 \pm 9.78 \times 10^{-12}$	$3.85 \pm 5.01 \times 10^{-11}$	-0.452	4.15×10^{-4}
	α .vs. F_I	$0.144 \pm 7.13 \times 10^{-12}$	$-1.647 \pm 5.05 \times 10^{-11}$	0.478	< 0.0001
2458539	α .vs. F_V	$-0.182 \pm 9 \times 10^{-3}$	$2.36 \pm 4.9 \times 10^2$	-0.326	2.06×10^{-3}
	α .vs. F_R	$0.158 \pm 8.9 \times 10^{-3}$	$0.319 \pm 5.8 \times 10^{-2}$	0.375	5.61×10^{-4}
	α .vs. F_I	$0.178 \pm 4.5 \times 10^{-3}$	$-0.255 \pm 4 \times 10^{-2}$	0.68	< 0.0001

Table 7 Linear Correlations of 3C 273 between F_ν and α

JD	α .vs. F_ν	$k \pm \Delta k$	$b \pm \Delta b$	r	p
2458539	α .vs. F_V	$(2 \pm 4) \times 10^{-3}$	-0.17 ± 0.115	0.0815	0.62184
	α .vs. F_R	$(-7 \pm 3.84) \times 10^{-3}$	0.691 ± 0.91	-0.31335	0.05208
	α .vs. F_I	$(-9.29 \pm 0.602) \times 10^{-3}$	0.1675 ± 0.0182	-0.93039	< 0.0001
2458540	α .vs. F_V	$(6.89 \pm 3.19) \times 10^{-3}$	-0.3 ± 0.079	0.3068	0.03594
	α .vs. F_R	$(0.949 \pm 2.6) \times 10^{-3}$	-0.151 ± 0.064	0.05252	0.72587
	α .vs. F_I	$(-7 \pm 0.464) \times 10^{-3}$	0.107 ± 0.0139	-0.92977	< 0.0001
2458541	α .vs. F_V	$5.24 \pm 2.55 \times 10^{-3}$	-0.259 ± 0.064	0.29224	0.04623
	α .vs. F_R	$(5.03 \pm 2.54) \times 10^{-3}$	-0.254 ± 0.063	0.28085	0.05316
	α .vs. F_I	$(-7.5 \pm 0.617) \times 10^{-3}$	0.098 ± 0.0186	-0.87338	< 0.0001
2458542	α .vs. F_V	$(8.6 \pm 1.7) \times 10^{-3}$	-0.34729 ± 0.04254	0.49339	< 0.0001
	α .vs. F_R	$(3.3 \pm 1.22) \times 10^{-3}$	-0.2126 ± 0.02947	0.29383	0.00816
	α .vs. F_I	$(-7.95 \pm 0.55) \times 10^{-3}$	0.111 ± 0.0168	-0.85145	< 0.0001

there are the following values, $\delta = 1.5$ (Guijosa & Daly 1996), $\delta = 2.1$ (Ghisellini et al. 1993), $\delta = 5.89$ (Yuan et al. 2017), $\delta = 8.76$ (Fan et al. 2009d), $\delta = 10.9$ (Hovatta et al. 2009), which are in the range from 1.5 to 8.76, and our result is in this coverage.

For 3C 273, based on the minimum $\Delta T = 0.107\text{h}$, $d_L = 734\text{ Mpc}$ (NED), $F_{\text{keV}} = 10.921\mu\text{Jy}$, $\alpha = 2.11$ (Brinkmann et al. 1997), $E_\gamma = 2.82\text{ GeV}$ (Fan et al. 2014), we can obtain $\delta \geq 6.04$. For a comparison, from the literatures, there are the following values, $\delta = 6$ (Hartman et al. 1999), $\delta = 6.64$ (Yuan et al. 2017), $\delta = 16.8$ (Savolainen et al. 2010), $\delta = 17$ (Hovatta et al. 2009), $\delta_{\text{VLBI}} = 5 \sim 12$ (Savolainen et al. 2006, Jorstad et al. 2005), which show the coverage of 6~17, and our result is in this range.

4.3 The Central Black Hole Mass

The central black holes play a key role in the observational properties of blazars and might shed some light on the evolution of active galactic nuclei (AGNs) (Fan 2005). The mass of black hole can be calculated by many methods, such as velocity dispersion (Wu et al. 2002; Woo & Urry 2002; Woo et al. 2005; Sbarato et al. 2012), reverberation mapping (Woo & Urry 2002), optical luminosity (Kawakatu et al. 2007), and so on.

For blazars, the origin of intra-day variability (IDV) periods are probably produced in the innermost regions

near the black hole, which can shed light on the emission size (R_{em}). This emission size (R_{em}) can be calculated as the following (Fan et al. 2018),

$$R_{\text{em}} \leq \frac{c\delta P}{1+z} = 1.08 \times 10^{14} \frac{\delta}{1+z} \left(\frac{P}{1\text{h}} \right) \text{cm}, \quad (11)$$

here, δ is Doppler factor, z is redshift, P is IDV period, c is light speed.

The IDV period can indicate the innermost stable orbit period, which depends on the black hole and the accretion disk (Xie et al. 2002, 2005; Dai et al. 2015; Liu & Bai 2015; Fan 2005; Fan et al. 2014). Based on the orbit period, we can obtain an upper limit to estimate the masses (M) of the central black hole (Abramowicz & Nobili 1982; Miller et al. 1989).

- (1) For a thin accretion disk surrounding a Schwarzschild black hole, $r = \frac{6GM}{c^2}$, the mass $M = 3.18 \times 10^5 \frac{P}{1+z} M_\odot$.
- (2) For a thick accretion disk surrounding a Schwarzschild black hole, $r = \frac{4GM}{c^2}$, the mass $M = 4.77 \times 10^5 \frac{P}{1+z} M_\odot$.
- (3) For a Kerr black hole ($a = 1$), $r = 1.48 \times 10^5 (1 + \sqrt{1 - a^2}) \frac{M}{M_\odot}$, the mass $M = 1.93 \times 10^6 \frac{P}{1+z} M_\odot$. Here, We use the IDV periods to indicate the period P .

For S5 0716+714, $\delta \geq 8.096$, the IDV period $P = 185.78 \pm 81.17\text{ min}$, the redshift $z = 0.31 \pm 0.08$ (Nilsson et al. 2008). So the black hole masses are in the range from $4.51 \times 10^7 M_\odot$ to $2.74 \times 10^8 M_\odot$, and emission size $R_{\text{em}} \leq 2.07 \times 10^{15}\text{ cm}$. Yuan et al. (2017) obtain the masses are in the range of $(4.2 \sim 25.6) \times 10^7 M_\odot$.

Gupta et al. (2009) obtained the mass $M = 2.5 \times 10^6 M_\odot$. Liu et al. (2019) obtained $R_{\text{em}} \leq 4.78 \times 10^{14}$ cm ($\delta = 10.8$). Our results are larger than the others. The main reason for this might be that we avail the IDV period (P) but the others use the minimum timescales (ΔT), which is lower than the IDV period.

For 3C273, IDV period $P = 60.09$ min, $z = 0.158$, $\delta \geq 6.04$, we obtain the central black hole mass in the range of $(1.65 \sim 10.0) \times 10^7 M_\odot$ and $R_{\text{em}} \leq 5.64 \times 10^{14}$ cm. For a comparison, Yuan et al. (2017) obtained the mass are in the range of $(0.95 \sim 5.74) \times 10^7 M_\odot$. Espaillat et al. (2008) obtained the black hole mass being about $M = 8.1 \times 10^7 M_\odot$. Liu et al. (2019) obtained $R_{\text{em}} \leq 6.27 \times 10^{14}$ cm ($\delta = 16.8$). Our black hole mass is consistent with Espaillat et al. (2008) and the emission region is consistent with Liu et al. (2019).

4.4 Relations Between Flux Densities and Spectral Indices

Based on our gross sample, not only for S5 0716+714, but also for 3C 273, F_ν and α show different correlations at different bands. With the frequency increasing ($V \rightarrow R \rightarrow I$), the correlation shows the following variation: strong anti-correlation \rightarrow weak or correlation \rightarrow no correlation or strong correlation.

To analyze their relations in more depth, we analyze their relations on every day, show the distributions of S5 0716+714 in Figure 12, and list all the fitting results in Tables 6 (S5 0716+714) and 7 (3C 273), where,

- Col. (1): JD;
- Col. (2): F_ν .vs. α , here $\nu = B, V, R, I$;
- Col. (3): $k \pm \Delta k$, the slope and the corresponding standard deviation;
- Col. (4): $b \pm \Delta b$, the intercept and the corresponding standard deviation;
- Col. (5): r , the correlative coefficient;
- Col. (6): p , the chance probability.

On every day, F_ν and α show different correlations for the two sources. For S5 0716+714, from V -band to I -band, the correlations show the variations of strong anti-correlation \rightarrow anti-correlation \rightarrow strong correlation. For 3C 273, the variation tendency is correlation or no correlation \rightarrow weak correlation \rightarrow strong anti-correlation.

4.5 Conclusions

In this work, we present $BVRI$ photometric results of S5 0716+714 and 3C 273 during the period from JD 2458536 to JD 2458542. Based on these observations, we come to the following conclusions.

Our results show that the trend between flux and spectrum is related to frequency not only for S5 0716+714 but also 3C 273. For S5 0716+714 the minimum time scale

is 0.31 hour, while 3C 273 is 0.36 hours. Both of them reflect periodicity. The former source may be periodicity, $P = 185.78$ min while the latter may be aperiodicity, $P = 60.09$ min, which should be verified by more data.

Furthermore, for S5 0716+714 we obtain the minimum time delay was $\tau_{RI} = 3.46$ min, for 3C 273 we obtain the minimum time delay was $\tau_{RI} = 6.42$ min.

Acknowledgements We acknowledge the support of the Yunnan Observatory 1.0m telescope. This work is partially supported by the National Natural Science Foundation of China (Grant Nos. U1831119, U1531245 and U1431112), Science and Technology Program of Guangzhou (201707010401).

References

- Abramowicz, M. A., & Nobili, L. 1982, Nature, 300, 506
- Agarwal, A., & Gupta, A. C. 2015, MNRAS, 450, 541
- Aller, H. D., Aller, M. F., Latimer, G. E., & Hodge, P. E. 1985, ApJS, 59, 513
- Begelman, M. C., Blandford, R. D., & Rees, M. J. 1980, Nature, 287, 307
- Bhatta, G., Webb, J. R., Hollingsworth, H., et al. 2013, A&A, 558, A92
- Blandford, R. D., & Königl, A. 1979, ApJ, 232, 34
- Bloom, S. D., & Marscher, A. P. 1996, ApJ, 461, 657
- Brinkmann, W., Yuan, W., & Siebert, J. 1997, A&A, 319, 413
- Camenzind, M., & Krockenberger, M. 1992, A&A, 255, 59
- Chakrabarti, S. K., & Wiita, P. J. 1993, ApJ, 411, 602
- Ciprini, S., Tosti, G., Raiteri, C. M., et al. 2003, A&A, 400, 487
- Ciprini, S., Takalo, L. O., Tosti, G., et al. 2007, A&A, 467, 465
- Collmar, W., Reimer, O., Bennett, K., et al. 2000, A&A, 354, 513
- Dai, B. Z., Li, X. H., Liu, Z. M., et al. 2009, MNRAS, 392, 1181
- Dai, B.-z., Zeng, W., Jiang, Z.-j., et al. 2015, ApJS, 218, 18
- de Diego, J. A. 2010, AJ, 139, 1269
- Deeming, T. J. 1975, Ap&SS, 36, 137
- Dennett-Thorpe, J., & de Bruyn, A. G. 2002, Nature, 415, 57
- Donato, D., Ghisellini, G., Tagliaferri, G., & Fossati, G. 2001, A&A, 375, 739
- Edelson, R. A., & Krolik, J. H. 1988, ApJ, 333, 646
- Espaillat, C., Bregman, J., Hughes, P., & Lloyd-Davies, E. 2008, ApJ, 679, 182
- Esposito, V., Walter, R., Jean, P., et al. 2015, A&A, 576, A122
- Fan, J.-H. 2005, ChJAA (Chin. J. Astron. Astrophys.), 5, 213S
- Fan, J. H., Kurtanidze, O., Liu, Y., et al. 2014, ApJS, 213, 26
- Fan, J. H., & Lin, R. G. 2000, ApJ, 537, 101
- Fan, J.-H., Yang, J.-H., Liu, Y., & Zhang, J.-Y. 2013, RAA (Research in Astronomy and Astrophysics), 13, 259
- Fan, J.-H., Yuan, Y.-H., Liu, Y., et al. 2009a, RAA (Research in Astronomy and Astrophysics), 9, 538
- Fan, J. H., Zhang, Y. W., Qian, B. C., Tao, J., et al. 2009b, ApJS, 181, 466
- Fan, J. H., Peng, Q. S., Tao, J., et al. 2009c, AJ, 138, 1428
- Fan, J. H., Huang, Y., He, T. M., et al. 2009d, PASJ, 61, 639

- Fan, J. H., Tao, J., et al. 2018, AJ, 155, 90
- Fan, J. H., Yuan, Y. H., et al. 2019, RAA (Research in Astronomy and Astrophysics), 19, 142
- Ghisellini, G., Padovani, P., Celotti, A., & Maraschi, L. 1993, ApJ, 407, 65
- Ghisellini, G., Tavecchio, F., Foschini, L., & Ghirlanda, G. 2011, MNRAS, 414, 2674
- Ghisellini, G., & Tavecchio, F. 2015, MNRAS, 448, 1060
- Ghosh, K. K., Ramsey, B. D., Sadun, A. C., & Soundararajaperumal, S. 2000, ApJS, 127, 11
- Guijosa, A., & Daly, R. 1996, ApJ, 461, 600
- Gupta, A. C., Fan, J. H., Bai, J. M., & Wagner, S. J. 2008, AJ, 135, 1384
- Gupta, A. C., Srivastava, A. K., & Wiita, P. J. 2009, ApJ, 690, 216
- Gupta, A. C., Krichbaum, T. P., Wiita, P. J., et al. 2012, MNRAS, 425, 1357
- Hartman, R. C., Bertsch, D. L., Bloom, S. D., et al. 1999, ApJS, 123, 79
- Heidt, J., & Wagner, S. J. 1996, A&A, 305, 42
- Hovatta, T., Valtaoja, E., Tornikoski, M., & Lähteenmäki, A. 2009, A&A, 494, 527
- Jorstad, S. G., et al., 2005, AJ, 130, 1418
- Kalita, N., Gupta, A. C., Wiita, P. J., Bhagwan, J., & Duorah, K. 2015, MNRAS, 451, 1356
- Kawakatu, N., Imanishi, M., & Nagao, T. 2007, ApJ, 661, 660
- Lee, J. W., Lee, S.-S., Kang, S., Byun, D.-Y., & Kim, S. S. 2016, A&A, 592, L10
- Liu, H. T., & Bai, J. M. 2015, AJ, 149, 191
- Liu, H. L., Feng, H. C., Xin, Y. X., et al. 2019, AJ, 880, 12
- Lomb, N. R. 1976, Ap&SS, 39, 447
- Man, Z., Zhang, X., Wu, J., & Yuan, Q. 2016, MNRAS, 456, 3168
- Mangalam, A. V., & Wiita, P. J. 1993, ApJ, 406, 420
- Mantovani, F., Junor, W., McHardy, I. M., & Valerio, C. 2000, A&A, 354, 497
- Maraschi, L., Ghisellini, G., & Celotti, A. 1992, ApJL, 397, L5
- Marscher, A. P., & Gear, W. K. 1985, ApJ, 298, 114
- Marscher, A. P., Jorstad, S. G., D'Arcangelo, F. D., et al. 2008, Nature, 452, 966
- Meng, N., Wu, J., Webb, J. R., Zhang, X., & Dai, Y. 2017, MNRAS, 469, 3588
- Miller, H. R. 1975, ApJL, 201, L109
- Miller, H. R., Carini, M. T., & Goodrich, B. D. 1989, Nature, 337, 627
- Nilsson, K., Pursimo, T., et al. 2008, A&A, 487, L29
- Oke, J. B. 1967, ApJ, 147, 901
- Poon, H., Fan, J. H., & Fu, J. N. 2009, ApJS, 185, 511
- Rani, B., Krichbaum, T. P., Fuhrmann, L., et al. 2013, A&A, 552, A11
- Rieger, F. M., & Mannheim, K. 2000, A&A, 359, 948
- Rieger, F. M., & Mannheim, K. 2003, A&A, 397, 121
- Romero, G. E., Cellone, S. A., & Combi, J. A. 1999, A&AS, 135, 477
- Sambruna, R. M., Urry, C. M., Tavecchio, F., et al. 2001, ApJL, 549, L161
- Sandrinelli, A., Covino, S., Dotti, M., & Treves, A. 2016, AJ, 151, 54
- Savolainen, T., Homan, D. C., Hovatta, T., et al. 2010, A&A, 512, A24
- Savolainen, T., Wiik, K., Valtaoja, E., & Tornikoski, M. 2006, A&A, 446, 71
- Sbarro, T., Ghisellini, G., Maraschi, L., & Colpi, M. 2012, MNRAS, 421, 1764
- Schulz, M., & Mudelsee, M., 2002, Computers & Geosciences, 28, 421
- Sillanpää, A., Haarala, S., Valtonen, M. J., et al. 1988, ApJ, 325, 628
- Smith, P. S., Balonek, T. J., Heckert, P. A., Elston, R., & Schmidt, G. D. 1985, AJ, 90, 1184
- Spangler, S., Fanti, R., Gregorini, L., & Padrielli, L. 1989, A&A, 209, 315
- Ulrich, M.-H., Maraschi, L., & Urry, C. M. 1997, ARA&A, 35, 445
- Urry, C. M., & Padovani, P. 1995, PASP, 107, 803
- Valtonen, M., Kidger, M., Lehto, H., & Poyner, G. 2008, A&A, 477, 407
- Villata, M., Raiteri, C. M., Lanteri, L., Sobrito, G., & Cavallone, M. 1998, A&AS, 130, 305
- Wagner, S. J., & Witzel, A. 1995, ARA&A, 33, 163
- Woo, J.-H., & Urry, C. M. 2002, ApJ, 579, 530
- Woo, J.-H., Urry, C. M., van der Marel, R. P., Lira, P., & Maza, J. 2005, ApJ, 631, 762
- Wu, J., Böttcher, M., Zhou, X., et al. 2012, AJ, 143, 108
- Wu, X.-B., Liu, F. K., & Zhang, T. Z. 2002, A&A, 389, 742
- Xie, G.-Z., Chen, L.-E., Xie, Z.-H., Ma, L., & Zhou, S.-B. 2005, PASJ, 57, 183
- Xie, G. Z., Li, K. H., Zhang, X., Bai, J. M., & Liu, W. W. 1999, ApJ, 522, 846
- Xie, G. Z., Liang, E. W., Xie, Z. H., & Dai, B. Z. 2002, AJ, 123, 2352
- Xie, G. Z., Zhou, S. B. et al. 2004, MNRAS, 348, 831
- Xiong, D. R., Bai, J. M., et al. 2017, ApJS, 229, 21
- Yuan, Y. H., Fan, J. H., & Pan, H. J., 2015a, AJ, 150, 67
- Yuan, Y. H., Fan, J. H., Pan, H. J., et al. 2015b, Ap&SS, 360, 9
- Yuan, Y. H., & Fan, J. H. 2015, Ap&SS, 357, 123
- Yuan, Y.-H., Fan, J.-h., Tao, J., et al. 2017, A&A, 605, A43
- Zdziarski, A. A., & Krolik, J. H. 1993, ApJL, 409, L33
- Zeng, W., Zhao, Q. J., Dai, B. Z., et al. 2018, PASP, 130, 024102
- Zhang, X., Zheng, Y. G., Zhang, H. J., et al. 2008, AJ, 136, 1846
- Zhang, Y. H. 2010, ApJ, 713, 180